Vol. 31 (2000) *ACTA PHYSICA POLONICA B* No 4

STRUCTURES AND CORRELATIONS IN IDEALLY ALIGNED POLAR GAY–BERNE SYSTEMS*

LECH LONGA[a,b], GRZEGORZ CHOLEWIAK[a] AND JOACHIM STELZER[a]

[a]Institute of Physics, Jagellonian University
Reymonta 4, 30-059 Kraków, Poland
[b]International Centre of Condensed Matter Physics, Universidade de Brasilia
Campus Universitário Darcy Ribeiro–CP 04513–CEP 70919-970
Brasilia-DF, Brazil

(Received January 24, 2000)

We study an ideally oriented system of Gay–Berne particles with embedded longitudinal dipole moments. While keeping the translational degrees of freedom of the molecules unrestricted we assume that their dipoles can be oriented either parallel or antiparallel to the positive z axis of the laboratory frame. At high temperatures, this frustrated Gay–Berne mesogen exhibits an ideally oriented nematic phase, which is the reference state of the system. In the limit of vanishing dipole moment nematic, smectic-A and smectic B phases are stable. Interestingly, by changing the magnitude and location of the molecular dipole in the nematic reference state we found dipole-induced smectic A, smectic B and tetragonal crystal phases, in addition to crystalline structures with smectic A_d and A_2-like dipolar organization. Various singlet, pair and triplet distribution functions were evaluated to elucidate short and long range organization in these phases. In particular, the importance of triplet correlations for a proper understanding of the structures and their local, dipolar organization is demonstrated.

PACS numbers: 61.30.Cz, 61.30.–v, 05.70.Ce, 02.70.Lq

1. Introduction

The relationship between the molecular interactions and the relative stability of the corresponding liquid crystalline phases is very intriguing and not yet fully understood. While it is widely accepted that shape anisotropy is a primary molecular ingredient to the formation of liquid crystals, experiments and theory indicate that the presence of dipolar groups could affect

---

[*] The work reported here was presented at the 17th International Liquid Crystal Conference, Strasbourg, France, July 19-24, 1998.

not only the relative stability and the range of the various liquid crystalline phases, but also their symmetry [1,2]. Evident examples are the smectic A phases, which are stabilized in systems with strong longitudinal dipole moments [1–4]. Their layer spacing ranges from l to $2l$. The most frequently observed among them is the A_d phase in which the layer spacing is typically $1.4\,l$, where l is the molecular length. Another one is the so called bilayer A_2 phase with layer spacing equal to $2l$, where each layer consists of two polarized sublayers with opposite direction of the dipoles. Also very interesting is the $\tilde{A}$ structure, often referred to as *antiphase*. It is built from A_2-like domains, which are arranged in a 2D centered rectangular lattice. The polarization of a single sublayer vanishes in this case.

The observation of the rich smectic A polymorphism inspired several theoretical studies which sought to explain the precise rôle dipolar forces can play in stabilizing polar smectics [4] and, in general, liquid crystalline phases [5,6]. In spite of the valuable insights gained the progress has been slow. This is, to a large extent, due to an oversimplified treatment of the electric dipole interaction, especially by density functional theories, where most often only two-body contributions have been considered [5]. Such approach disregards the frustration effect [4], which could only be accounted for by including higher than binary correlations (see *e.g.* discussion in [6,7]).

More specifically, two longitudinal dipole moments attain the energetically most stable configuration in an antiparallel arrangement, which is consistent with two-body theories that support strong short-range antiferroelectric correlations in polar liquids. But when we consider a third dipole approaching the other two dipoles, we note that it does not find any favorable orientation. Namely, if it is antiparallel to one it must be parallel to the other, which is the energetically least stable configuration for two dipoles. We say that it becomes frustrated. Hence an ensemble of dipoles in a fluid state seeks for an optimal arrangement, which usually is different from that dictated by a two-body analysis [4].

A direct and reliable way to account for many-body correlations induced by dipolar forces are computer simulations. They provide a valuable tool to investigate liquid crystalline ordering arriving from particular molecular interactions. To estimate the effects that can result from dipolar interactions it seems of particular importance to study relatively simple models for which the case of vanishing dipole is well understood. One such model is represented by dipolar spherocylinders, which have been studied intensively by computer simulations [8–13]. In particular, it was shown that the smectic A phase is stabilized with respect to the nematic phase for the systems with central dipoles, but that terminal dipoles enhance the stability of nematics.

Shape anisotropy is only one of the two major molecular factors responsible for the existence of liquid crystals. The second one are the attractive forces, which always exist between real molecules. Hence, to study the effect of dipole moments on the stability of liquid crystalline phases it seems essential that model interactions are of the form where both these factors are available. One of the potentials fulfilling this condition and being remarkably successful for the computer modeling of liquid crystalline molecules is the single site, anisotropic pair potential of Lennard-Jones type, developed by Gay and Berne (GB) [14]. The potential contains four parameters, two of them measuring the anisotropy in shape and interaction energy of a pair of uniaxial molecules (see Section 2). Using molecular dynamics and Monte Carlo techniques a rich phase behaviour of the four-parameter Gay–Berne homologues has been found [15–21]. For example, with its original set of parameters the Gay–Berne system stabilizes isotropic, nematic and smectic B phases [17]. The observed phases and the phase transitions between them resemble those found for real mesogens. In view of this success the original Gey–Berne potential has been developed further to include biaxiality [22], flexibility [23], more complex molecules composed of a collection of Gay–Berne sites [24] and dipolar forces [25–32].

As concerning the polar GB potentials some numerical results have been offered. Satoh *et al.* [25–27] have carried out Monte Carlo simulations of 256 Gay–Berne molecules with central and terminal, longitudinal dipole moments. With canonical NVT ensemble (constant number of particles, volume and temperature) and the reaction field method [33,34] to treat dipolar interactions they observed the formation of isotropic, nematic, smectic and crystalline phases. For central dipoles [25] they found that the isotropic–nematic transition temperature is not sensitive to the strength of the dipole moment, whereas the nematic–smectic A phase transition is slightly shifted to higher temperatures as the strength of dipole moment is increased.

For terminal dipoles [26] the transition temperature from the isotropic to the nematic phase is shifted towards higher temperatures and the temperature range of the nematic phase is broadened with increasing dipole moment. Additionally, for strong dipole moments a tetragonal crystalline structure is observed [27]. In view of relatively small system size and lack of test on the rôle of boundary conditions these predictions, especially for smectic and solid phases, should be regarded as preliminary. Note that the system size dependence was seen for dipolar hard-core systems when the number of particles was less than 512 [35].

Houssa *et al.* [28] have studied dipolar GB systems with original values of the GB parameters [14,17] at reduced temperature $T^* = 1.25$, again utilizing the reaction field method. The systems contained 256 molecules with axial dipole moments located at the centre of the molecule. Though the number of molecules also was comparably small, they partly compensated this by performing constant pressure NPT Monte Carlo simulations. They found only an isotropic–smectic B transition, whereas in the absence of dipolar interactions the system has isotropic, nematic and smectic B phases at the same temperature. In their most recent studies [29] they extended simulations to determine phase diagrams and the structure of the mesophases. The latter was inferred from a set of reduced singlet and pair distribution functions.

Very interesting structures were found by Berardi *et al.* [30]. They have used NVT Monte Carlo simulations to study large polar GB systems ($N = 1000$ and $N = 8000$ molecules), also with central and terminal longitudinal dipole moments. The energy of dipolar interactions has been calculated with the help of an alternative method, the Ewald summation technique [34, 36]. They showed that monolayer smectic A liquid crystals and modulated smectic $\tilde{A}$ domains could be stabilized in both cases. The molecules in the smectic phases were almost perfectly aligned.

In our calculations we performed canonical (NVT) Monte Carlo simulations for relatively large systems of $N = 648$ GB molecules with embedded longitudinal dipole moments (some tests were performed for $N = 2592$). The dipolar energy was calculated with the help of very reliable, but time consuming Ewald summation technique. We investigated the influence of the dipole strength and the dipole location in the molecule on the formation of smectic A and higher ordered phases, and studied dipolar correlations in these phases. In particular, a very accurate information about the structure of the mesophases and the way system deals with frustration has been provided by analysing *triplet* distribution functions. These functions were calculated together with singlet- and pair-distributions.

As the Ewald technique requires enormous computing time we simplified the model by assuming an ideal nematic order. That is, we considered only translational and dipole flip MC moves, which should be accurate enough to analyze polar structures that occur on the background of nematic ordering. Indeed, for polar GB mesogens the orientational order in such phases was found to be very high [30]. This simplification was also necessary to get a clear picture of short range dipolar correlations, especially triplet ones.

Summarizing, the objectives of the present studies are the following: First to consider in detail the relation between the strength and position of the longitudinal dipole moment on the formation of mesophases. Not only central and terminal, but also intermediate positions of the dipoles are considered. Secondly, to take care of a possible dependence on system size and simulation box geometry, and to use very accurate Ewald summation technique for dipolar interactions. Finally, to provide a detailed characterization of the phases in terms of singlet, pair and triplet distribution functions.

We should mention that due to the presence of frustration effect the triplet correlations are of particular importance for a proper understanding of dipolar organization in liquid crystals [6]. Yet, they have not been studied for liquid crystals. The only papers dealing with triplet correlations we are aware of are those by McNeil *et al.* [37] and Fushiki [38] for Lennard–Jones fluids of spherically symmetric particles. While, in general, triplet correlations are extremely difficult to analyze, it will be demonstrated that the problem is feasible for the case of ideal orientational order.

The present paper is arranged as follows. In Section 2, we define the model and give essential details of the Monte Carlo simulations. The distribution functions are introduced in Section 3, while the results of the simulations and the structure analysis are presented in Section 4. Section 5 is devoted to a summary and some final conclusions.

2. Model and simulation method

We consider prolate uniaxial molecules with point dipole moments parallel to the long molecular axis. The intermolecular pair potential is chosen to take the form of an anisotropic single site continuous potential,

$$V = V_{\mathrm{GB}} + V_{dd}, \tag{1}$$

where V_{GB} is the Gay–Berne (GB) potential [14] and V_{dd} represents the dipole-dipole interaction. The GB potential is a generalization of the standard 12–6 Lennard-Jones potential to molecules of uniaxial symmetry. It depends on the unit vectors $\hat{\boldsymbol{e}}_i$ and $\hat{\boldsymbol{e}}_j$ describing the orientations of a pair of molecules and on the separation vector $\boldsymbol{r} = \boldsymbol{r}_i - \boldsymbol{r}_j$ of their centers of mass $\boldsymbol{r}_i$ and $\boldsymbol{r}_j$. The detailed expressions are

$$V_{\mathrm{GB}}(\hat{\boldsymbol{e}}_i, \hat{\boldsymbol{e}}_j, \boldsymbol{r}) = 4\,\epsilon(\hat{\boldsymbol{e}}_i, \hat{\boldsymbol{e}}_j, \hat{\boldsymbol{r}})\,\left(R^{-12} - R^{-6}\right), \tag{2}$$

where

$$R = \frac{[r - \sigma(\hat{\boldsymbol{e}}_i, \hat{\boldsymbol{e}}_j, \hat{\boldsymbol{r}}) + \sigma_0]}{\sigma_0}\,. \tag{3}$$

Here $r = |\boldsymbol{r}|$ is the length of the separation vector and $\hat{\boldsymbol{r}} = \boldsymbol{r}/r$ is its orientation.

The orientation dependent molecular shape parameter σ and the energy parameter ϵ are defined by the following set of equations:

$$\sigma(\hat{\boldsymbol{e}}_i, \hat{\boldsymbol{e}}_j, \hat{\boldsymbol{r}}) = \sigma_0\,\left(1 - \tfrac{1}{2}\chi\left[\frac{(\hat{\boldsymbol{r}}\cdot\hat{\boldsymbol{e}}_i + \hat{\boldsymbol{r}}\cdot\hat{\boldsymbol{e}}_j)^2}{1 + \chi\,(\hat{\boldsymbol{e}}_i\cdot\hat{\boldsymbol{e}}_j)} + \frac{(\hat{\boldsymbol{r}}\cdot\hat{\boldsymbol{e}}_i - \hat{\boldsymbol{r}}\cdot\hat{\boldsymbol{e}}_j)^2}{1 - \chi\,(\hat{\boldsymbol{e}}_i\cdot\hat{\boldsymbol{e}}_j)}\right]\right)^{-1/2}, \tag{4}$$

$$\epsilon(\hat{\boldsymbol{e}}_i, \hat{\boldsymbol{e}}_j, \hat{\boldsymbol{r}}) = \epsilon^{\nu}(\hat{\boldsymbol{e}}_i, \hat{\boldsymbol{e}}_j)\,\epsilon'^{\mu}(\hat{\boldsymbol{e}}_i, \hat{\boldsymbol{e}}_j, \hat{\boldsymbol{r}})\,, \tag{5}$$

and

$$\epsilon(\hat{\boldsymbol{e}}_i, \hat{\boldsymbol{e}}_j) = \epsilon_0\,\left[1 - \chi^2\,(\hat{\boldsymbol{e}}_i\cdot\hat{\boldsymbol{e}}_j)^2\right]^{-1/2}, \tag{6}$$

$$\epsilon'(\hat{\boldsymbol{e}}_i, \hat{\boldsymbol{e}}_j, \hat{\boldsymbol{r}}) = 1 - \tfrac{1}{2}\chi' \left[\frac{(\hat{\boldsymbol{r}} \cdot \hat{\boldsymbol{e}}_i + \hat{\boldsymbol{r}} \cdot \hat{\boldsymbol{e}}_j)^2}{1 + \chi' \, (\hat{\boldsymbol{e}}_i \cdot \hat{\boldsymbol{e}}_j)} + \frac{(\hat{\boldsymbol{r}} \cdot \hat{\boldsymbol{e}}_i - \hat{\boldsymbol{r}} \cdot \hat{\boldsymbol{e}}_j)^2}{1 - \chi' \, (\hat{\boldsymbol{e}}_i \cdot \hat{\boldsymbol{e}}_j)} \right] . \tag{7}$$

The parameters χ and χ' are related to the length-to-breadth ratio κ and potential well depths ratio κ' for the side-to-side and end-to-end arrangements. They read

$$\chi = \frac{\kappa^2 - 1}{\kappa^2 + 1}, \qquad \chi' = \frac{\kappa'^{1/\mu} - 1}{\kappa'^{1/\mu} + 1}. \tag{8}$$

As already discussed in the previous section this generic potential describes quite well liquid crystal formation in thermotropic materials [15–21].

Among the cases analysed the original GB model [14], defined by $\kappa = 3$, $\kappa' = 5$, $\mu = 2$ and $\nu = 1$, is the one most thoroughly studied [15–17]. Its potential energy contours for the long molecular axes parallel to each other are shown in Figure 1(a). Obviously, the potential prefers a side-to-side arrangement of the pair of molecules which, in turn, promotes liquid crystallinity. The length-to-breadth ratio is 3:1, as the value of κ suggests, and this seems to be the minimum value that is found experimentally for molecules forming liquid crystals. The complete phase diagram for this model is found in [17]. It is particularly simple, revealing only vapour, isotropic liquid, nematic and smectic B phases.

We have investigated a generalized version of this model by adding to the GB potential in Eq. (2) a point dipolar interaction V_{dd} due to a permanent dipole moment $\boldsymbol{\mu}$,

$$V_{dd}(\boldsymbol{r}, \boldsymbol{\mu}_i, \boldsymbol{\mu}_j) = \frac{\boldsymbol{\mu}_i \cdot \boldsymbol{\mu}_j - 3(\boldsymbol{\mu}_i \cdot \hat{\boldsymbol{\rho}})(\boldsymbol{\mu}_j \cdot \hat{\boldsymbol{\rho}})}{\rho^3} , \tag{9}$$

where $\boldsymbol{\rho} = \boldsymbol{r} + d\,(\hat{\boldsymbol{e}}_i - \hat{\boldsymbol{e}}_j)$ is the relative position of the dipole moments of two molecules. In the present studies the direction of the dipole moment is assumed to coincide with the long molecular axis ($\boldsymbol{\mu}_i = \mu\,\hat{\boldsymbol{e}}_i$), whereas its location on the molecular axis is given by a parameter d, which denotes the distance of the dipole from the molecular center. Modifications of the potential energy contours due to the presence of the dipole moments are shown in Figs. 1(b)–(d).

We have performed extensive NVT Monte Carlo simulations [34] of a system of $N = 648$ molecules confined to a tetragonal box and subject to periodic boundary conditions and minimum image convention [34]. Some testing runs have been carried out for $N = 2592$ molecules. The particles were assumed to interact according to the polar GB potential, Eq. (1), where the strength μ and position d of the dipole moment were treated as parameters. The GB potential was cut at $r_{\mathrm{cut}} = 4.0\,\sigma_0$ and shifted.

Our primary objective was to investigate in a systematic way the influence of dipolar forces on the formation of orientationally and spatially

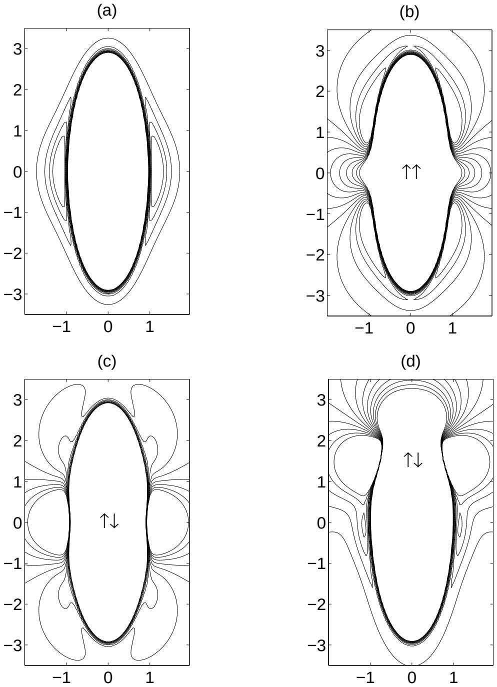

Fig. 1. The potential energy contours calculated for a pair of Gay–Berne particles with embedded longitudinal dipole moments. The molecules are assumed to be parallel to the z axis of the laboratory frame. The contours are parametrized by the strength, the position and the orientation (indicated by arrows) of the dipole moments: (a) — $\mu^* = 0$; (b) — $\mu^* = 2.5$, d^* - arbitrary, ↑↑ dipole configuration; (c) — $\mu^* = 2.5$, $d^* = 0$, ↑↓ dipole configuration; (d) — $\mu^* = 2.5$, $d^* = 0.75$, ↑↓ dipole configuration. The innermost contours correspond to potential energy 2.0 and the other contours are for values of the scaled potential energy decreasing in steps of 0.25. In this figure and in all figures that follow quantities with asterisk are given in reduced units introduced in the Appendix A.

ordered liquid crystalline phases, like orthogonal smectic phases. As the orientational order parameter in the smectic phases of the polar GB system is known to be close to its saturation value of 1.0 [30], we assumed an ideal nematic order approximation. This means that all molecular long axes were fixed parallel to the director, which coincided with the $\hat{\boldsymbol{z}}$ axis. Although the orientations were frozen, the molecules still preserved all translational degrees of freedom and their dipole moments were allowed to flip, as in the Ising model. Therefore in our simulations a Monte Carlo attempted move consisted of shifting the center of mass of a particle or flipping its dipole. The step size $[\delta x, \delta y, \delta z]$ for the center of mass move was fixed such that overall acceptance ratio did not exceed 40%. The initial configuration for each run was taken to be (a) a hexagonal lattice of ideally oriented molecules with randomly distributed dipoles, (b) a translationally disordered ideal nematic configuration and, most frequently, (c) the final configuration of a Monte Carlo simulation at slightly different values for the strength and location of the dipole moment. The system was relaxed to equilibrium until the configurational energy and distribution functions showed no systematic changes with the MC steps (usually between $4 \cdot 10^4$ and 10^5 cycles). Tests for about $5 \cdot 10^5$ cycles were also performed occasionally. After the equilibration process the system was further simulated for an additional 10^5 MC cycles, and every tenth cycle the configuration was saved for a subsequent analysis of distribution functions.

In simulations dipole-dipole interactions require a special treatment due to their long range. Here the energy of the dipolar interactions was calculated using the Ewald summation technique [34, 36] with tin foil boundary conditions characterized by a dielectric constant $\epsilon = 1$. This is the standard choice in this type of calculations and it represents a vacuum surrounding the system at large distances. The choice of the boundary conditions may have significant influence on the results (*e.g.* conducting *vs.* vacuum boundary conditions [11]). Detailed expressions concerning the Ewald sum are listed in Appendix B. The convergence parameter γ was taken $5.75/L_{\min}$, where $L_{\min} = \min(L_x, L_y, L_z)$ and L_x, L_y, L_z denote the dimensions of the simulation box. With this choice of γ the real space part of the Ewald sum can be limited to the central box and the Fourier space part may be restricted to vectors $\boldsymbol{k} = (2\pi n_x/L_x,\ 2\pi n_y/L_y,\ 2\pi n_z/L_z)$ such that $|\boldsymbol{n}| = \sqrt{n_x^2 + n_y^2 + n_z^2} \leq 6$.

During the simulations the density and the temperature were fixed to the values $\rho^* = 0.335$ and $T^* = 2.8$, respectively, where all quantities are expressed in reduced units defined in Appendix A. This choice of the temperature corresponds in our model to a stable nematic state in the absence of dipoles. Some additional runs have been performed for $T^* = 2$.

Calculations for various dipole strengths and locations were performed. We considered three different values of the dipole moment: $\mu^* = 1.5$, 2.0, 2.5. In the first simulation, the dipole moments were assumed to vanish, thus providing the nonpolar reference system. For nonzero values of μ^* the dipole was positioned at $d^* = 0$, 0.75 and 1, relative to the center of the molecule. Thus, the first and the last case correspond to central and (nearly) terminal dipoles, respectively. For the intermediate value of d^* the dipole was positioned half way between the center and end of the molecule. However, please be aware of the fact that the molecular length is not precisely defined for soft interactions. Actually, if we define the molecular shape as one corresponding to zero energy contour for a pair of molecules with their long axes parallel to each other then the molecules studied here are of length 3.

Still a few comments concerning Monte Carlo simulations with dipolar interactions seems in place. First of all, for relatively large systems the computational requirements are enormous as compared to the case with short range interactions. This is due to the very reliable, but time consuming Ewald procedure [11, 36]. Very recently Houssa *et al.* [28, 29] argued that the Ewald method could safely be replaced by the reaction field method, the latter being much less computer time demanding. They provided some checks for states with dipolar disorder. However, we are not aware of any such studies for structures with long range dipolar ordering and therefore we prefer to use the Ewald method.

Finally, a constant volume simulation is not the best choice to study structures with translational order. It may happen, especially for small systems, that the actual equilibrium structure does not fit to the assumed simulation box [28]. This problem can be avoided when allowing the box volume to fluctuate, which is realized in practice in isothermal-isobaric or constant pressure (NPT) Monte Carlo simulations. Although this could readily be done the presence of the long-range potential causes that the $\boldsymbol{k}$-vectors of the Ewald summation and the term $\frac{\exp(-k^2/4\gamma^2)}{k^2}$ entering the expressions, (see Appendix B), must be recalculated for each new simulation box, which, in turn considerably extends the simulation time. For this reason we limited ourselves to the NVT MC scheme. In order to check against the dependence of the results on the simulation box, some trial runs with $N = 2592$ molecules have been carried out. Additionally, the dimensions of the simulation box (with particles inside) were rescaled subject to constant density, which guaranteed better adjustment of the resulting structures.

3. Structure of the phases

All simulations were performed for those state points of the phase diagram where the restricted GB potential stabilizes a nematic phase. The remaining stable phase of the ideally oriented GB we have found for our parameters is smectic B. Thus, any stabilization of other smectic or crystal phases must be attributed to the dipolar interactions. The equilibrium structure of the emerging phases can be quantified by the probability densities for finding one, two, three, or more molecules at specified location and orientation in phase space. These probabilities can be extracted from the simulation data. Here we restrict ourselves to singlet, pair and triplet distribution functions.

3.1. Singlet distribution function

The simplest of the distribution functions is the longitudinal singlet distribution [20]. It allows to study smectic ordering along the director. More specifically, we define the longitudinal one-particle distribution function $P(s,z)$ for the ideal nematic order approximation as

$$P(s,z)=\frac{L_z}{N}\left\langle\sum_{i=1}^{N}\delta_{s,s_i}\,\delta(z-z_i)\right\rangle=\frac{1}{2}\left[g^{(1)}(z)+s\,\sigma^{(1)}(z)\right], \tag{10}$$

where $s=\pm1$, $s_i=\pm1$ ($\boldsymbol{\mu}_i=\mu\,\hat{\boldsymbol{e}}_i$, $\boldsymbol{e}_i=s_i\,\hat{\boldsymbol{z}}$).

In the expression (10) we introduced the profile of the particle density $g^{(1)}(z)$ and the profile of the dipole density $\sigma^{(1)}(z)$, both measured along the smectic layer normal, *i.e.,* parallel to the $\hat{\boldsymbol{z}}$ axis. They read

$$g^{(1)}(z)=\frac{L_z}{N}\left\langle\sum_{i=1}^{N}\delta(z-z_i)\right\rangle\ , \tag{11}$$

$$\sigma^{(1)}(z)=\frac{L_z}{N}\left\langle\sum_{i=1}^{N}s_i\,\delta(z-z_i)\right\rangle. \tag{12}$$

Additionally, we introduce smectic and dipolar order parameters. Their definitions follow from the Fourier expansion of $P(s,z)$ and are given by

$$P(s,z)=1+2\sum_{n=0}\zeta_{2n+1}\,s\,\cos\left[(2n+1)qz\right]+2\sum_{n=1}\tau_{2n}\,\cos\left(2nqz\right). \tag{13}$$

In (13) $q=\frac{\pi}{l}$ is the wavelength of the smectic structure, l being the layer spacing. The Fourier amplitudes τ_{2n} and ζ_{2n+1} are the smectic order parameters and dipolar order parameters, respectively. For the structures emerging from the simulations we evaluate only the leading, lowest order amplitudes ζ_1 and τ_2. They are determined from the magnitude of the main peaks in the Fourier transformations of particle density (11) and dipole density (12), respectively, and are evaluated as averages, independent of the system of frame,

$$\zeta_1=\underset{\{l\}}{\mathrm{Max}}\ \left|\langle s\exp(\pi iz/l)\rangle\right|\ , \tag{14}$$

$$\tau_2=\underset{\{l\}}{\mathrm{Max}}\ \left|\langle\exp(2\pi iz/l)\rangle\right|\ . \tag{15}$$

The same procedure can be used to find higher order amplitudes of the singlet distribution function (10).

Long range positional order in smectic planes can be probed with the help of the in-plane one-particle distribution, defined as

$$P_\perp(s,\boldsymbol{r}_\perp) = 1 + \sum_{{}^*\boldsymbol{k}} \frac{1}{\sqrt{N_{{}^*\boldsymbol{k}}}} \left[\tau_\perp({}^*k) + \zeta_\perp({}^*k)\, s\right] \sum_{\boldsymbol{k}\in{}^*\boldsymbol{k}} e^{i\boldsymbol{k}\cdot\boldsymbol{r}_\perp}, \tag{16}$$

where the set ${}^*\boldsymbol{k}$ of the two-dimensional wave vectors $\boldsymbol{k}$ of the same moduli is taken from the reciprocal lattice representing in-plane symmetry (*i.e.* the symmetry of a two-dimensional cut perpendicular to $\hat{\boldsymbol{z}}$) and $N_{{}^*\boldsymbol{k}}$ denotes the number of $\boldsymbol{k}$ vectors in ${}^*\boldsymbol{k}$. Note that some of the amplitudes $\zeta_\perp({}^*k)$ may vanish. As an example, to be discussed in detail in the present paper, consider the nonpolar crystalline smectic B structure. In this case the in-plane symmetry is that of the triangular lattice and the leading order parameter $\tau_\perp({}^*k) \equiv \tau_\perp$ is associated with the following set ${}^*\boldsymbol{k}$ of six $\boldsymbol{k}$ vectors:

$$\boldsymbol{k}_1 = \tfrac{1}{a}\left[-\hat{\boldsymbol{x}} - \tfrac{\sqrt{3}}{3}\hat{\boldsymbol{y}}\right],\ \boldsymbol{k}_2 = \tfrac{\sqrt{3}}{3a}\hat{\boldsymbol{y}},\ \boldsymbol{k}_3 = \tfrac{1}{a}\left[\hat{\boldsymbol{x}} - \tfrac{\sqrt{3}}{3}\hat{\boldsymbol{y}}\right],\ \boldsymbol{k}_4 = -\boldsymbol{k}_1,\ \boldsymbol{k}_5 = -\boldsymbol{k}_2$$

and $\boldsymbol{k}_6 = -\boldsymbol{k}_3$. Here a is the lattice spacing, $\hat{\boldsymbol{x}}$ is the unit vector along the x axis and $\hat{\boldsymbol{y}}$ is the unit vector along the y axis. Again $\tau_\perp$ can be evaluated as an average, independent of the system of frame,

$$\tau_\perp = \operatorname*{Max}_{\{a,\psi\}} \left| \sum_{\beta=1}^{6} \langle \exp\left(i\boldsymbol{k}_\beta\cdot(\mathcal{R}(\psi)\boldsymbol{r}_\perp)\right)\rangle \right|, \tag{17}$$

where $\mathcal{R}(\psi)$ is a global rotation about the z axis by angle ψ.

3.2. Pair distribution function

The general pair distribution function [39] of a liquid crystal phase composed of uniaxial rigid molecules is a complex quantity, both to calculate and to represent graphically (see *e.g.* [20] and references therein). However, the situation is considerably simplified for ideal nematic order. In this case the pair distribution function $g^{(2)}$ of polar liquid crystals can be introduced in many equivalent ways as

$$\begin{aligned} g^{(2)} &\equiv g^{(2)}(\boldsymbol{r}, s_1\hat{\boldsymbol{z}}, s_2\hat{\boldsymbol{z}}) = \frac{V}{N^2}\left\langle \sum_i \sum_{j\neq i} \delta_{s_1 s_i}\delta_{s_2 s_j}\delta(\boldsymbol{r} - \boldsymbol{r}_i + \boldsymbol{r}_j)\right\rangle \\ &\equiv g^{(2)}(r_\perp, \phi, z, s_1 s_2) \end{aligned} \tag{18}$$

$$= \frac{V}{N^2 r_\perp}\left\langle \sum_i \sum_{j\neq i} \delta_{s_1 s_i}\delta_{s_2 s_j}\delta(r_\perp - |\boldsymbol{r}_i - \boldsymbol{r}_j|_\perp)\delta(\phi - |\phi_i - \phi_j|)\delta(z - z_i + z_j)\right\rangle$$

$$= g^{(2)}(r, \hat{\boldsymbol{r}}\cdot\hat{\boldsymbol{z}}\,, s_1 s_2) = \sum_L \frac{2L+1}{2}\, g_L^{(2)}(r, s_1 s_2) P_L(\cos\theta)\,, \tag{19}$$

where P_L are Legendre polynomials, θ is the angle between the unit vector $\hat{\boldsymbol{r}} \equiv \hat{\boldsymbol{r}}_{12} = \boldsymbol{r}_{12}/r_{12} \equiv \boldsymbol{r}/r$ and where $\hat{\boldsymbol{z}}$, and $r_\perp$, ϕ, z are the cyllindrical coordinates of $\boldsymbol{r}$. It gives the probability that one particle with dipole orientation s_1 is separated by a distance $\boldsymbol{r}$ from another with dipole s_2 (irrespective of their absolute positions), relative to the probability expected for a completely random distribution at the same density.

This distribution gives the exact representation for pair correlations of translationally invariant phases. Also note that the Legendre polynomial expansion of $g^{(2)}$ is very simple as compared to the general case.

There are two pair distribution functions that can be derived from $g^{(2)}$, which are of particular importance in exploring the layer structure of a phase. One is the axial pair distribution functions (APDF), $g_{||}^{(2)}(z, s_1 s_2)$, defined as

$$\begin{aligned} g_{||}^{(2)}(z, s_1 s_2) &= \frac{L_z}{V}\int_0^{2\pi} d\phi \int_0^{\infty} r_\perp dr_\perp\; g^{(2)}(r_\perp, \phi, z, s_1 s_2) \\ &= \frac{L_z}{2N^2}\left\langle \sum_i \sum_{j\neq i} \delta_{s_1 s_i}\,\delta_{s_2 s_j}\,\delta(z - |z_i - z_j|)\right\rangle . \end{aligned} \tag{20}$$

It gives the probability of finding two centers of mass of particles at a resolved, relative distance of z along the director, and with orientations s_1, s_2 of the molecular dipoles relative to the same probability calculated for an ideal gas of particles at the same density. We calculate $g_{||}^{(2)}(z, \uparrow\uparrow)$ for pairs of molecules with the same dipolar orientations and $g_{||}^{(2)}(z, \uparrow\downarrow)$ for pairs of molecules with their dipoles oriented in opposite directions, where $s = 1 \equiv\uparrow$ and $s = -1 \equiv\downarrow$. From these two functions we then obtain $g_{||}^{(2)}(z)$ for arbitrary orientation of the dipoles using relation

$$g_{||}^{(2)}(z) = \sum_{s_1, s_2} g_{||}^{(2)}(z, s_1 s_2) = 2\, g_{||}^{(2)}(z, \uparrow\uparrow) + 2\, g_{||}^{(2)}(z, \uparrow\downarrow), \tag{21}$$

which follows directly from the "up-down" symmetry of the Hamiltonian.

Similarly, the structure perpendicular to the director can be probed with the Transversal Pair Distribution Function (TPDF), $g_\perp^{(2)}(r_\perp, s_1 s_2)$, where $r_\perp$

is the separation between the centers of mass of particles projected onto a plane orthogonal to $\hat{\boldsymbol{z}}$. It is defined by

$$g_{\perp}^{(2)}(r_{\perp}, s_1 s_2) = \frac{1}{4\pi D} \int\limits_{0}^{2\pi} \mathrm{d}\phi \int\limits_{-D}^{D} \mathrm{d}z \; g^{(2)}(r_{\perp}, \phi, z, s_1 s_2)$$

$$= \frac{V}{4\pi r_{\perp} D N^2} \left\langle \sum_{i} \sum_{j \neq i} \delta_{s_1 s_i} \, \delta_{s_2 s_j} \, \delta(r_{\perp} - |\boldsymbol{r}_i - \boldsymbol{r}_j|_{\perp}) \, \Theta(D - |z_i - z_j|) \right\rangle , \tag{22}$$

where $\Theta(x)$ denotes the Heaviside step function, and where D is a small parameter ($D^* \approx 0.5$). Note that we may also regard $\boldsymbol{r}_i$ and $\boldsymbol{r}_j$ in the Eq. (18) as positions of the dipole moments. In this case we get another interesting TPDF, which shows the tendency for the dipoles to gather in plane. So defined TPDF is also of interest for polar systems and will be calculated in our simulations.

Again, we evaluate $g_{\perp}^{(2)}(r_{\perp}, \uparrow\uparrow)$ and $g_{\perp}^{(2)}(r_{\perp}, \uparrow\downarrow)$, for parallel and opposite dipolar orientations, respectively, and $g_{\perp}^{(2)}(r_{\perp})$, for arbitrary orientation of the dipoles. The latter function is defined as

$$g_{\perp}^{(2)}(r_{\perp}) = \sum_{s_1, s_2} g_{\perp}^{(2)}(r_{\perp}, s_1 s_2) = 2\, g_{\perp}^{(2)}(r_{\perp}, \uparrow\uparrow) + 2\, g_{\perp}^{(2)}(r_{\perp}, \uparrow\downarrow). \tag{23}$$

Also we have calculated the degree of hexatic order by expanding the general $g_{\perp}(\boldsymbol{r}_{\perp})$ in an angular Fourier series

$$g_{\perp}^{(2)}(\boldsymbol{r}_{\perp}) \equiv \frac{1}{2D} \sum_{s_1 s_2} \int\limits_{-D}^{D} g^{(2)}(\boldsymbol{r}, s_1 \hat{\boldsymbol{z}}, s_2 \hat{\boldsymbol{z}}) = g_{\perp}(\overline{r}_{\perp}) \sum_{n} \Psi_{6n}(\overline{r}_{\perp}) \, \exp\left(i \, 6 n \phi_{jk}\right), \tag{24}$$

where $\overline{r}_{\perp}$ is equal to the average in-plane nearest neighbour separation and ϕ_{jk} is the angle that the separation vector $\boldsymbol{r}_j - \boldsymbol{r}_k$ between neighbouring molecules j and k makes with the x axis. Then, the leading hexatic order parameter is given by

$$\Psi_6 = \left| \left\langle \frac{1}{N_{nn}} \sum_{j} \sum_{(k,j)} \exp\left(i \, 6 \phi_{jk}\right) \right\rangle \right| , \tag{25}$$

where (k, j) denotes summation over molecules j that are the nearest neighbours of the molecule k and where $N_{nn} = \sum_j \sum_{(k,j)} 1$. In selecting the nearest neighbours we considered molecules separated by $\overline{r}_\perp \pm \delta$ with δ being the distance from $\overline{r}_\perp$, where the magnitude $g_\perp(\overline{r}_\perp)$ of the leading peak of $g_\perp(r_\perp)$ halves. Normalization in (25) is such that for an ideal triangular lattice $\Psi_6 = 1$.

3.3. Triplet distribution function

The thermodynamic properties usually depend not only on singlet and pair distribution functions but also on higher distributions, in particular, on triplet one [39], even when the model potential does not contain direct three body interactions. As argued in Section 1, the Triplet Distribution (TD) should be of particular importance for strongly polar liquid crystals, where frustration plays an important rôle. Although the TD is straightforward to evaluate in simulations [39] it has not been analysed for liquid crystals so far. Also results for simpler, spherically symmetric systems, are scarce. Actually the only work on *ab initio* calculation of triplet distributions we are aware of is that of McNeil *et al.* [37], where results for an ordinary Lennard-Jones fluid are reported. This is probably due to the fact that the general spherical expansion for the triplet distribution is quite involved and the calculation of averages is time consuming. Even for relatively small systems the number of triplet configurations to be analysed in one cycle is quite large. For example, in simulations with $N = 648$ the number of triplets equals $N(N-1)(N-2)/6 = 45139896$ (!). Also the visualization of triplet correlations, even if we manage to count triplets, is a nontrivial task.

For ideally oriented dipolar systems the triplet distribution function $g^{(3)}$ is defined as

$$\begin{aligned} g^{(3)} &\equiv g^{(3)}(\boldsymbol{r},\boldsymbol{r'},s_1s_2s_3) = \frac{V^2}{N^3}\Big\langle \sum_i \sum_{j\neq i} \sum_{k\neq j\neq i} \delta_{s_1s_i}\delta_{s_2s_j}\delta_{s_3s_k} \\ &\quad \times\delta(\boldsymbol{r}-\boldsymbol{r}_j+\boldsymbol{r}_i)\delta(\boldsymbol{r'}-\boldsymbol{r}_k+\boldsymbol{r}_i)\Big\rangle \\ &= \frac{V^2}{r_\perp {r'}_\perp N^3}\Big\langle \sum_i \sum_{j\neq i} \sum_{k\neq j\neq i} \delta_{s_1s_i}\delta_{s_2s_j}\delta_{s_3s_k}\delta(r_\perp - |\boldsymbol{r}_j+\boldsymbol{r}_i|_\perp) \\ &\quad \times\delta(\phi-\phi_j+\phi_i)\delta(z-z_j+z_i) \\ &\quad \times\delta({r'}_\perp - |\boldsymbol{r}_k+\boldsymbol{r}_i|_\perp)\delta(\phi'-\phi_k+\phi_i)\delta(z'-z_k+z_i)\Big\rangle, \end{aligned} \tag{26}$$

where the last part of the formula (26) is given in cylindrical coordinates. Next, we introduce the in-plane part $g^{(3)}_\perp$ of $g^{(3)}$, which counts only these triplets that lie in planes perpendicular to the director and form triangles where two of the three sides are r and r' with θ being the angle between them. It reads

$$
\begin{aligned}
g_{\perp}^{(3)}(r_{\perp}, r'_{\perp}, \theta, s_1 s_2 s_3) &= \frac{1}{8\pi D^2} \int\limits_{-D}^{D} \mathrm{d}z \int\limits_{-D}^{D} \mathrm{d}z' \int\limits_{0}^{2\pi} \mathrm{d}\phi \int\limits_{0}^{2\pi} \mathrm{d}\phi' \\
&\times \delta(\theta - \mathrm{Min}(|\phi - \phi'|, 2\pi - |\phi - \phi'|))\ g^{(3)}(\boldsymbol{r}, \boldsymbol{r'}, s_1 s_2 s_3) \\
&= \frac{V^2}{8\pi r_{\perp} r'_{\perp} D^2 N^3} \Big\langle \sum_i \sum_{j \neq i} \sum_{k \neq j \neq i} \delta_{s_1 s_i} \delta_{s_2 s_j} \delta_{s_3 s_k} \\
&\times \delta(r_{\perp} - |\boldsymbol{r}_j + \boldsymbol{r}_i|_{\perp}) \delta({r'}_{\perp} - |\boldsymbol{r}_k + \boldsymbol{r}_i|_{\perp}) \\
&\times \Theta(D - |z_j - z_i|) \Theta(D - |z_k - z_i|) \delta(\theta - \mathrm{Min}(|\phi_j - \phi_k|, 2\pi - |\phi_j - \phi_k|)) \Big\rangle .
\end{aligned}
\tag{27}
$$

To simplify the analysis further we restrict ourselves to triplets forming isosceles triangles. That is, we study the case when $r = r'$ in Eq. (27) and introduce notation $g_{\perp}^{(3)} \equiv g_{\perp}^{(3)}(r_{\perp}, r_{\perp}, \theta, s_1 s_2 s_3) \equiv g_{\perp}^{(3)}(r_{\perp}, \theta, s_1 s_2 s_3)$. Owing to the nature of the model studied we think that other configurations do not contribute in an essential way to quantitative understanding of triplet correlations. As for TPDF two cases are considered. The first one assumes that the vectors $\boldsymbol{r}_i$, $\boldsymbol{r}_j$, and $\boldsymbol{r}_k$ in (26) refer to the centers of mass of the molecules. In the second case these vectors are assumed to parametrize positions of the dipole moments. Thus $g_{\perp}^{(3)}$ accounts for tendency of the three centers of mass or, in the second case, of the three dipole moments to gather in planes perpendicular to the director. Also please note that $g_{\perp}^{(3)}$ averaged over θ is proportional to $[g_{\perp}^{(2)}]^2$, which could be used to check consistency of the calculations.

Now we turn to technical aspects of the calculations. First of all we need to identify the isosceles configurations. This is done with the help of the algorithm used in work [37]. Namely, for a given molecule i we calculate the minimum image separations $r_{ij} \equiv |\boldsymbol{r}_{ij}| = |\boldsymbol{r}_i - \boldsymbol{r}_j|$ from the $N - 1$ remaining molecules, discretize it and store the results in the `distij` table. For the same i we also evaluate the minimum image vectors $\boldsymbol{r}_{ij}$ and save their components in arrays `distijx`, `distijy` and `distijz`. If pairs i, j do not belong to the same plane normal to the director, the corresponding matrix element `distij[j]` is set to zero. By definition, particles i, j are associated with a plane provided that $|z_i - z_j| < D$.

Search for isosceles triangles starts by sorting the `distij` array in ascending order. This is done in practice by introducing a permutation matrix `perm` of particle indices j such that `distij[perm[j]]` gives a sorted matrix. The identification of the triangles starts from the first index `m` for which `distij[perm[m]]`>0. The triangle is found when the two elements `distij[perm[n]]` and `distij[perm[n+1]]` (`n` $\geq$ `m`) are equal (up to $\pm D$). Finally, we compute the angle θ between $\boldsymbol{r}_{ij}$ and $\boldsymbol{r}_{ik}$, where j=`perm[n]` and k=`perm[n+1]` and $r_\perp = r_{ij} = r_{ik}$. The procedure described above must be applied to all molecules of the system.

As already indicated before, the triplet distribution $g_\perp^{(3)}$ is parametrized by $(r_\perp, \theta)$. Moreover we will distinguish three nonequivalent dipole configurations: $s_1s_2s_3 = \uparrow\uparrow\uparrow$, $\uparrow\uparrow\downarrow$ and $\uparrow\downarrow\downarrow$, and compute separately three distribution functions $g_\perp^{(3)}(r_\perp, \theta, s_1s_2s_3)$: $g_\perp^{(3)}(r_\perp, \theta, \uparrow\uparrow\uparrow)$, $g_\perp^{(3)}(r_\perp, \theta, \uparrow\uparrow\downarrow)$ and $g_\perp^{(3)}(r_\perp, \theta, \uparrow\downarrow\downarrow)$, where the dipole moment s_1 refers to the nonequivalent vertex of isosceles triangle. They are connected by the relation:

$$g_\perp^{(3)}(r_\perp, \theta) \equiv \sum_{s_1,s_2,s_3} g_\perp^{(3)}(r_\perp, \theta, s_1s_2s_3) = 2g_\perp^{(3)}(r_\perp, \theta, \uparrow\uparrow\uparrow) + 4g_\perp^{(3)}(r_\perp, \theta, \uparrow\uparrow\downarrow) + 2g_\perp^{(3)}(r_\perp, \theta, \uparrow\downarrow\downarrow), \tag{28}$$

which results from *global* up-down symmetry of pair interactions and symmetry with respect to exchange of s_2 and s_3 in Eq. (26). Please note that the exhange symmetry is not obeyed by the dipole moment s_1.

Applying the same procedure to an ideal gas of molecules with density ρ yields normalization $N_{r\theta}^{\rm ideal} = 2\pi\delta\theta N(2rD\delta r\rho)^2$, where $N_{r\theta}^{\rm ideal}$ is associated with the histogram element $(r,\ r+\delta r)$, $(\theta,\ \theta+\delta\theta)$. We compute $g_\perp^{(3)}(r_\perp, \theta)$ as $N_{r\theta}/N_{r\theta}^{\rm ideal}$.

4. Results and discussion

Most of the simulations were carried out for an ensemble of 648 molecules but some runs with $N = 2592$ were performed to ensure that the results obtained were not significantly dependent on system size. The temperature and density were fixed to $T^* = 2.8$ and $\rho^* = 0.335$, respectively. In discussing the results we shall also refer to the parameter $\alpha = \langle E_{dd}\rangle / \langle E_{\rm tot}\rangle$, where $\langle E_{\rm tot}\rangle$ is the average potential energy of the system and $\langle E_{dd}\rangle$ is the average energy of the dipolar interactions.

The simulations start with the nonpolar case ($\mu^* = 0$) for which we obtained an ideally oriented nematic phase. In this phase the smectic order parameter τ_2, Eq. (15), should vanish. But due to system size τ_2 is not precisely zero ($\tau_2 = 0.025$).

The pair distribution functions $g_L^{(2)}(r^*, s_1s_2)$ (Fig. 2) and $g_\perp^{(2)}$ (Fig. 3) also do not reveal any long range order and they have the characteristic features

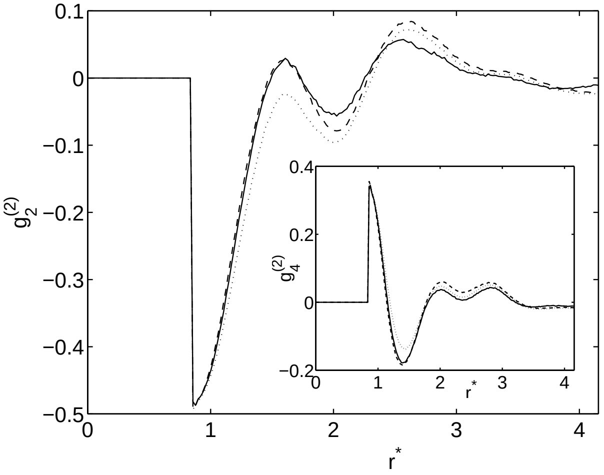

Fig. 2. The pair distribution functions $g_L^{(2)}(r^*)$ for $L = 2$ in the nematic phase of nonpolar molecules (continuous line) and $g_L^{(2)}(r^*, s_1s_2)$ in the smectic A phase of molecules with central dipole moment $\mu^* = 1.5$. The dotted line represents the $s_1s_2 =\uparrow\downarrow$ case while the dashed one corresponds to $s_1s_2 =\uparrow\uparrow$ dipole configurations. The inset shows the same cases, but for $L = 4$.

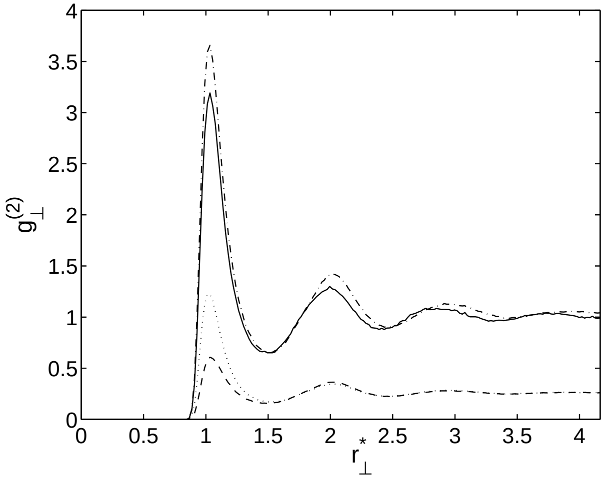

Fig. 3. The transversal pair distribution functions $g_\perp^{(2)}(r_\perp^*)$ in the nematic phase of nonpolar molecules (continuous line) and $g_\perp^{(2)}(r_\perp^*, s_1, s_2)$ in the smectic A phase of molecules with central dipole moment $\mu^* = 1.5$. The dash-dotted line represents the total distribution function, $g_\perp^{(2)}(r_\perp^*)$, while dotted and dashed cases correspond to $s_1s_2 =\uparrow\downarrow$ and $s_1s_2 =\uparrow\uparrow$ configurations, respectively.

of liquid structure. As expected, the correlations are the strongest when the distance vector between molecular centers is perpendicular to $\hat{\boldsymbol{z}}$ (negative values of $g_2^{(2)}$ and positive values of $g_4^{(2)}$ at short distances in Fig. 2). This corresponds to the first peak of $g_\perp^{(2)}$ (Fig. 3). Short range character of the pair correlations, as displayed in Figs. 2 and 3, agrees qualitatively with what we observe for unconstrained nematics (see *e.g.* [20] and references therein). But neither orientational correlation coefficients $\{g_L^{(2)}, L = 0, 2, 4, ...\}$, Eq. (18), nor $g_\perp^{(2)}$ compare directly with analogous functions determined for unconstrained nematics [20]. The reason is that in the latter case usually all information about the relative orientation between the director and other vectors involved is averaged out.

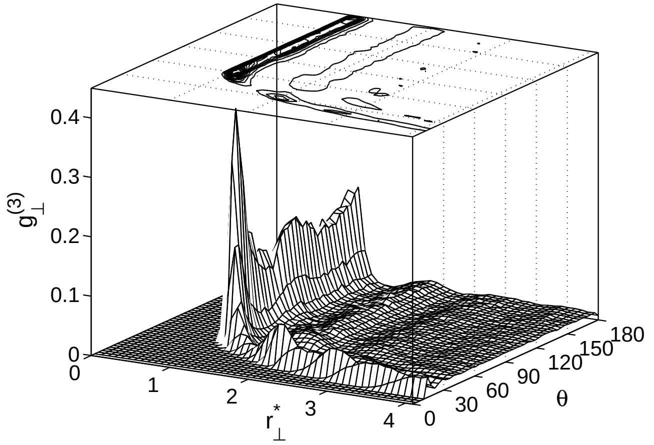

Fig. 4. The triplet distribution function $g_\perp^{(3)}(r_\perp^*, \theta)$ of the nonpolar, ideally oriented Gay–Berne system in the nematic phase. Note that the angle θ is given in degrees. That is why $g_\perp^{(3)}$ tends to $\pi/180$ at large distances.

The triplet distribution function (Fig. 4) provides a deeper insight into short range organization, especially into the 'fine structure' of the leading peak of $g_\perp^{(2)}$. It shows that the major contribution to this peak comes from triplets forming equilateral triangles (maximum of $g_\perp^{(3)}$ at $\theta = 60°$), and from triplets of particles placed equally along a straight line (second, broad maximum of $g_\perp^{(3)}$ at $\theta = 180°$). Also there exists a third weak maximum of $g_\perp^{(3)}$ at $\theta = 120°$. These maxima suggest that the nonpolar system under study locally supports a weak hexagonal ordering and linear correlations of triplets in the nematic state. As we shall see these local correlations will be strenthened or converted into tetragonal ones depending on the position and value of the dipole moment.

Given this characterization of the reference phase we now turn to the systems with nonzero dipole moment. We start with the dipoles localized at the molecular center ($d^* = 0$). For $\mu^* = 1.5$ the ratio of the average dipole-dipole energy to the total energy yields $\alpha = 23\%$. The density modulation along the director is now clearly established, giving $\tau_2 = 0.11$. We attribute this to a (weak) dipole-induced smectic A structure. The layer spacing, l^*, is about 2.7, indicating that the layers are slightly interdigitated. As in the nematic phase, the pair distributions, Figs. 2 and 3, are fluid-like. Within the layers the dipoles are distributed randomly as in the smectic A phase and they show no long-range ordering. This could again be deduced from Figs. 2 and 3. At short distances, however, the in-plane correlations are dominated by *up–down* configurations (Fig. 3). The 'fine structure' of these correlations can again be studied with the help of the triplet in-plane distribution function. First, the dipole averaged distribution function, Eq. (23), appears similar to the nematic one (Fig. 4), again displaying local hexagonal structure and linear correlations of the triplets. A good approximation for this function can be obtained from the nematic one (Fig. 4) by multiplying the latter by the factor of 1.5. The leading peak of these correlations is again dominated by the triplets occupying equilateral triangles and, hence, it belongs to frustrated configurations. Indeed, this observation is supported by dipole dependent triplet correlations, Figs. 5a and 5b, which show that the peak at 60° is due to the triplets where one dipole moment is oriented in the opposite direction of the two others. Interestingly, the contribution from non-frustrated triplets, where the middle dipole has different orientation than the terminal ones, becomes equally important (see peaks at 120° and 180° in Fig. 5(b)). The distribution function where all three dipoles are oriented in the same direction shows the same structure of the peaks as Fig. 5(b), but is approximately six times smaller.

An increase of magnitude of the central dipole to $\mu^* = 2.0$ causes a new structure to appear. The density profile now reveals distinct, well organized smectic layers, yielding a smectic order parameter of $\tau_2 = 0.8$ (see Table I), which is close to its saturation value of 1. Even though α exceeds 37% in this case, no long-range dipolar order along the layers is stabilized. This is clear from the APDFs, (Fig. 6), which show strong axial correlations. These correlations are independent on the relative dipolar orientations of the pairs of the molecules, rendering the functions $g_{||}^{(2)}(z^*, \uparrow\uparrow)$ (dashed curve in Fig. 6) and $g_{||}^{(2)}(z^*, \uparrow\downarrow)$ (dotted curve in Fig. 6) almost identical.

Inspection of $g_{\perp}^{(2)}(r_{\perp}^*)$ (Fig. 7) and $g_{\perp}^{(3)}(r_{\perp}^*, \theta, s_1 s_2 s_3)$ (Figs. 8(a), 8(b) and 8(c)) shows that the system has developed positional correlations within each layer. This is especially clear from the dipole-dependent $g_{\perp}^{(3)}$ functions, Figs. 8(a), 8(b) and 8(c), where these correlations are shown to be of the

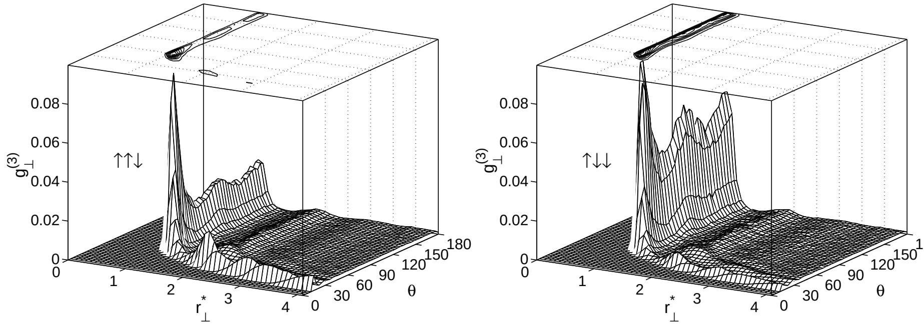

Fig. 5. The triplet distribution function $g_\perp^{(3)}(r_\perp^*, \theta, s_1 s_2 s_3)$ of polar, ideally oriented Gay–Berne system in the smectic A phase for (a) — $s_1 s_2 s_3 =\uparrow\uparrow\downarrow$ and (b) — $s_1 s_2 s_3 =\uparrow\downarrow\downarrow$. The dipolar strength and the dipole location are $\mu^* = 1.5$ and $d^* = 0$, respectively.

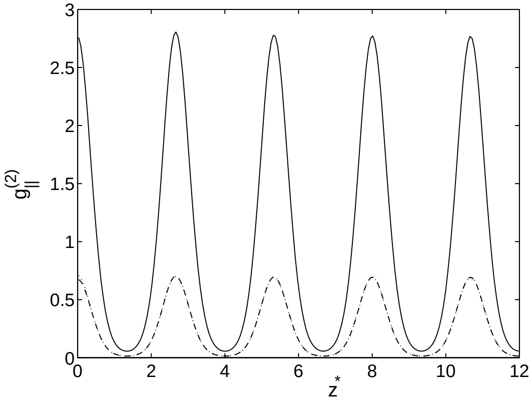

Fig. 6. The axial pair distribution function $g_{||}^{(2)}(z^*, s_1 s_2)$ in the smectic B phase. The dipolar strength and the dipole location are $\mu^* = 2$ and $d^* = 0$, respectively. The solid line represents dipole-averaged total distribution function $g_{||}^{(2)}(z^*)$ and the dashed line is for the $s_1 s_2 =\uparrow\uparrow$ distribution. The dotted line gives the $s_1 s_2 =\uparrow\downarrow$ distribution.

hexagonal type. Hence, we have strong indication that this new phase is a mesogenic smectic B (S_B) phase. It is known that S_B can exist as a crystalline B phase ($S_{\mathrm{cr}B}$) with AAA and ABC stacking as well as the more common ABAB, or as a hexatic $S_{\mathrm{hex}B}$ phase [40]. All these phases are built from in-plane hexagons formed by the centers of mass of the molecules. The hexagons are, on average, parallel to each other, giving a nonzero value of the hexatic order parameter (24). In the case of the $S_{\mathrm{cr}B}$ phase they additionally occupy the sites of a two-dimensional, hexagonal lattice, resulting in

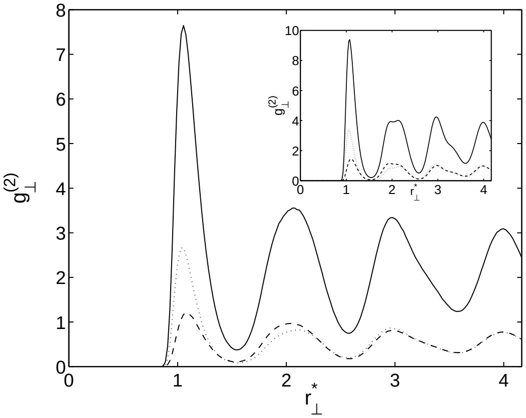

Fig. 7. The transversal pair distribution function, $g_\perp^{(2)}(r_\perp^*, s_1 s_2)$, in the smectic B phase of polar molecules with central dipole moment $\mu^* = 2$. The continuous line represents the total distribution function, $g_\perp^{(2)}(r_\perp^*)$, while dotted and dashed lines correspond to $s_1 s_2 = \uparrow\downarrow$ and $s_1 s_2 = \uparrow\uparrow$ cases, respectively. The inset shows the transversal distribution in the same phase, but for $T^* = 2$.

a long-range in-plane positional order, which is *absent* in the hexatic phase. Unfortunately, it decays slowly with the system size, making distinction between $S_{\mathrm{hex}B}$ and $S_{\mathrm{cr}B}$ in simulations rather subtle (see *e.g.* [17]).

Our simulation results are consistent with two possibilities for this phase: $S_{\mathrm{cr}B}$ with ABAB stacking or $S_{\mathrm{hex}B}$, where the first option seems more likely. We started the analysis of in-plane ordering by calculating the order parameters $\tau_\perp$, Eq. (17), and Ψ_6, Eq. (25), which were found to be 0.38 and 0.69, respectively, while the maximal value of both is 1 for the ideal triangular lattice. However, the order parameter $\tau_\perp$ vanishes when calculated for the total system ($\tau_\perp = 0.02$), indicating that different smectic layers are either uncorrelated or shifted with respect to each other. By analyzing both possibilities we found that the layers are likely to form an ABAB stacking and interdigitate. The average in-plane position of a randomly chosen molecule coincides with the center of a triangle formed by the average positions of the nearest-neighbour triplets in adjacent layers. The bulk value of $\tau_\perp$ for the ABAB stacking (after taking into account the relative phase shift between the neighbouring layers) is found to be $\tau_\perp = 0.23$. This is considerably lower than the (small) in-plane value, which indicates on high disorder not only in atomic positions within the hexagonal layers but also in the stacking of the layers.

Both in-plane and bulk $\tau_\perp$ are much smaller than what one would expect for a first order phase transition between smectic A (nematic) and crystalline

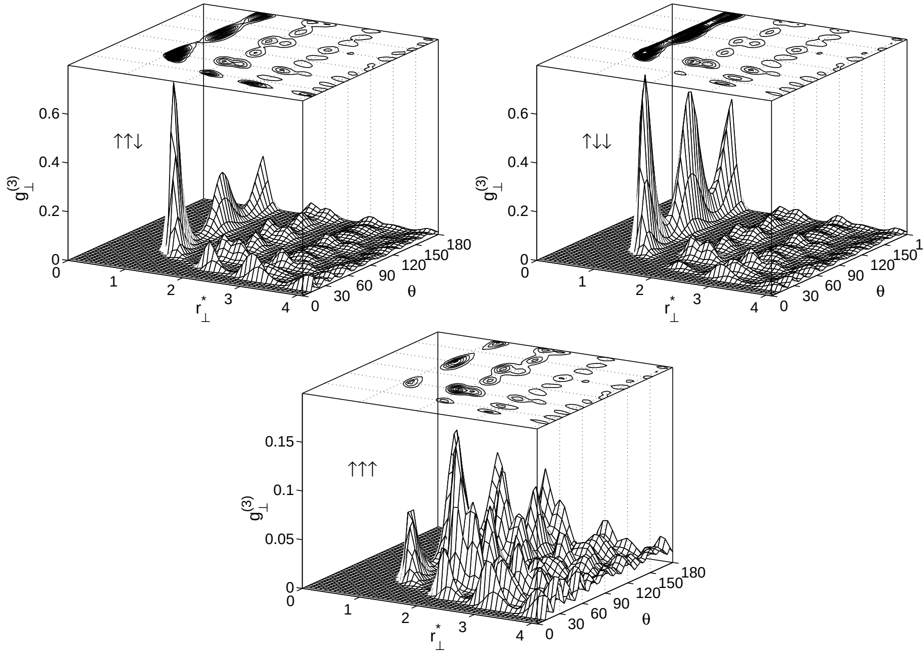

Fig. 8. The triplet distribution function $g_\perp^{(3)}(r_\perp^*, \theta, s_1 s_2 s_3)$ of polar, ideally oriented Gay–Berne system in the smectic B phase: (a) — the $s_1 s_2 s_3 = \uparrow\uparrow\downarrow$ case; (b) — the $s_1 s_2 s_3 = \uparrow\downarrow\downarrow$ case, and (c) — the $s_1 s_2 s_3 = \uparrow\uparrow\uparrow$ case. The dipolar strength and the dipole location are $\mu^* = 2$ and $d^* = 0$, respectively.

smectic B. Note also that $g_\perp^{(2)}$ (Fig. 7) and $g_\perp^{(3)}$, Figs. 8a, 8b and 8c, are dominated by the nearest neighbour peaks at $r_\perp^* \approx 1.1$. The second and the third peak of the TPDF are approximately of the same height, but weak and broad in comparison to the first one. Actually each of them is composed of two peaks, although they cannot be resolved at $T^* = 2.8$. Their existence becomes obvious at $T^* = 2$, which is shown as inset in Fig. 7.

While hexagonal in-plane arrangement cannot be justified by looking at $g_\perp^{(2)}$ it becomes apparent when we switch to triplet correlations (see Figs. 8a, 8b and 8c). In particular, we observe that all three first-order peaks occurring at scaled separations, $r_\perp^*$, of approximately 1.1 and angles, θ, of 60°, 120° and 180° are now well-resolved. Qualitatively they follow the same trends as previously observed peaks for $\mu^* = 1.5$. Interestingly, the secondary peaks at $r_\perp^*$ between 2 and 3 are also better resolved, but their amplitudes are more than four times smaller than those of the leading one.

The qualitative difference between the correlations for the system with $\mu^* = 0, 1.5$ and 2 prompt us to conclude that the phase for $\mu^* = 2$ is most probably a smectic B although it is rather difficult to choose between hexatic and crystalline smectic B ordering. The existence of the ABAB stacking and of a similar structure for even higher central dipole moment ($\mu^* = 2.5$) or lower temperature, $T^* = 2.0$, (see inset in Fig. 7) makes, in our opinion, the crystalline case more likely. This is in line with the very recent studies by Satoh *et al.* [27], who also claim to have stable dipolar S_B phase, most probably of AA or AB stacking, although this aspect of the ordering has not been studied.

On the other hand the frustration mechanism seems to be in favour of the hexatic arrangement. More specifically, a triangular lattice of dipole moments is completely frustrated and hence energetically unfavourable. Introduction of in-plane defects or imperfections, which destroy long-range hexagonal order, could help in overcoming this difficulty, especially for strong dipole moments.

We now analyse the systems where the dipole is shifted by $d^* = 0.75$. For molecules with dipole moments of magnitude $\mu^* = 1.5$ ($\alpha = 36\%$) the layered structure is stabilized without long-range dipolar order along the z axis. The small value of the translational order parameter ($\tau_2 \approx 0.35$) would indicate that this structure is probably smectic A. But the situation seems more subtle. First of all, the most probable relative distance between the positions of the molecular centers along the z direction is found to be 1.7, which means that the layers are strongly interdigitated. Clearly, this is aided by the presence of the dipole moments as the dipole-dipole interaction for a pair of molecules is minimized for antiparallel configuration when the reduced distance between the molecular centers is of 1.5. To understand the averaged molecular arrangement more thoroughly, it would be necessary to examine the transversal distributions of the molecules within a single layer and within the planes of the dipole moments, which we have done. The results are somewhat surprising because we found that the strongest transversal pair correlations (and hence also the triplet ones) are *not* for in-plane centers of mass but for in-plane antiparallel dipole moments with the corresponding centers of mass of the molecules being located in the neighbouring layers (see Fig. 9). Interestingly, the leading peak of $g_\perp^{(2)}$ at $r_\perp^* \approx 0.9$ is exclusively built from molecular units (pairs, triplets, *etc.*) that yield better, local compensation of the dipolar interactions. This should be contrasted with the much weaker peak at $r_\perp^* \approx 1.06$ of the in-layer correlations (inset in Fig. 9). The probability of finding in-plane parallel dipoles at short separations is smaller by a factor of 7. To clarify the origin of the leading peak of $g_\perp^{(2)}$ in Fig. 9, the strongest ($s_1 s_2 s_3 = \uparrow\downarrow\downarrow$) and total triplet dipole correlations, calculated in the plane of dipoles, are shown in Figs. 10(a) and 10(b), respectively. These correlations are essentially dominated by two broad peaks at 90° and 180°. For comparison we showed the

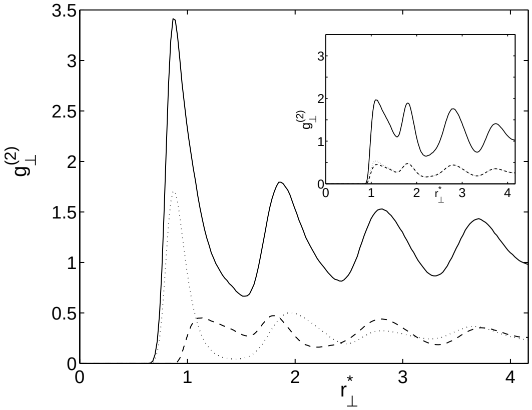

Fig. 9. The transversal pair distribution function, $g_\perp^{(2)}(r_\perp^*, s_1s_2)$, in the smectic A phase of polar molecules with dipole moment $\mu^* = 1.5$ positioned at $d^* = 0.75$. The distribution is shown for the case when the dipole moments lay in plane perpendicular to director. The molecular centers are localized in the neighbouring layers. The continuous line represents the total distribution function, $g_\perp^{(2)}(r_\perp^*)$; dotted and dashed lines correspond to $s_1s_2 =\uparrow\downarrow$ and $s_1s_2 =\uparrow\uparrow$ cases, respectively. The inset shows the transversal distribution in the same phase but viewed from the smectic plane of molecular centers. Note that the dashed lines representing parallel orientations of the dipole moments are the same in both cases.

triplet $s_1s_2s_3 =\uparrow\uparrow\uparrow$ correlations in Fig. 10(c). They again appear weaker by a factor of 7 than the leading $s_1s_2s_3 =\uparrow\downarrow\downarrow$ correlations. The remaining $s_1s_2s_3 =\uparrow\uparrow\downarrow$ triplet distribution function is about 5 times smaller than that for $s_1s_2s_3 =\uparrow\downarrow\downarrow$ configurations.

Combining these results with the in-layer center of mass triplet distribution, Fig. 10(d), we see that there may be two possible scenarios explaining the results. The first possibility is that the phase is a (weak) crystalline smectic with interdigitated, tetragonal layers ($S_{\mathrm{cr}T}$). The layer spacing and the dipolar ordering between the neighbouring layers is such that the dipolar energy is minimized due to weak polymer-like configurations. But the apparently very small probability to have in-plane molecules with parallel dipole moments at reduced distance of $0.9 \times \sqrt{2}$ (see Fig. 10(c)) and the structure of correlations shown in Figs. 9 and 10a suggests that the phase could also be crystalline one of a smectic A_d-type. Then the layers would be supported by in-plane 'branched polymer-like structures' with the layer spacing being $2l^* \approx 3.4$. Interestingly, for $d^* = 0.75$ the local hexagonal ordering of central dipoles is transformed into an unfrustrated tetragonal one.

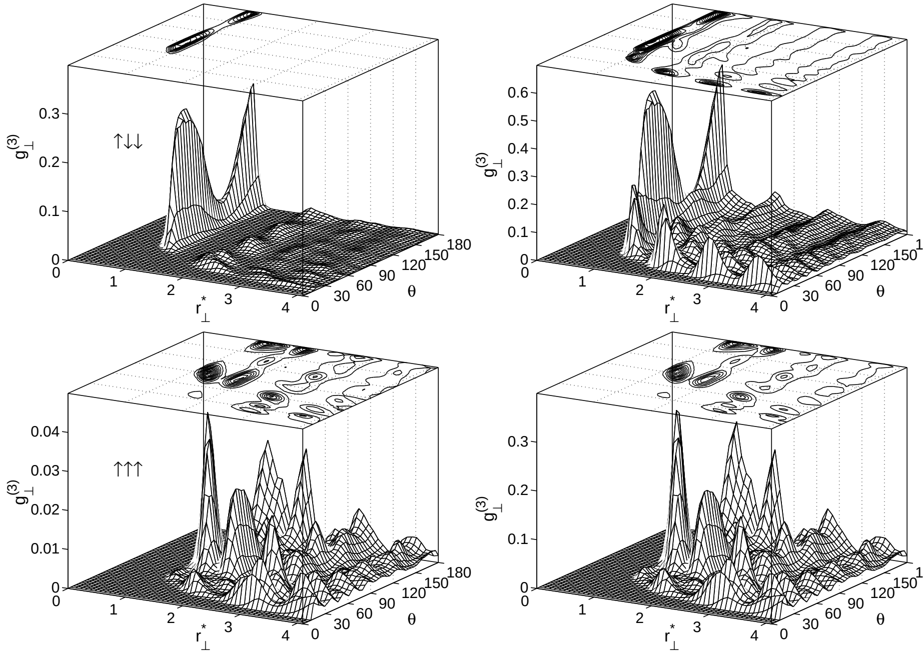

Fig. 10. The triplet distribution function $g_\perp^{(3)}(r_\perp^*, \theta, s_1 s_2 s_3)$ of polar, ideally oriented Gay–Berne system in the smectic phase of local tetragonal symmetry within layers: *(a)* in the plane of ↑↓↓-oriented dipole moments (this case shows the strongest dipolar correlations between the dipoles; note that the centers of mass of the molecules with oppositely oriented dipole moments belong to the neighbouring layers); *(b)* total distribution function for the case *(a)*; *(c)* in-layer, $s_1 s_2 s_3 =$↑↑↑ distribution function, and *(d)* in-layer center of mass total distribution function. The dipolar strength and the dipole location are $\mu^* = 1.5$ and $d^* = 0.75$, respectively.

For dipole moments of magnitude $\mu^* = 2$ the peaks of the distribution functions become sharper and their fine structure could be resolved (see *e.g.* Figs. 11a and 11b). The order parameter τ_2 is now of 0.55. This we attribute to crystalline smectic ordering of tetragonal symmetry, similar to that one reported very recently by Satoh [27]. The square base lies within the smectic layers (Fig. 12). Though the influence of the dipolar interactions is much stronger now ($\alpha = 56\%$), still no long-range dipolar order has been found for this case. But enhancement of the ↑↑↑ triplet correlations by a factor of 2.5 (compare Figs. 10c and 11b) indicates that further increase of the dipole strength may yield a crystalline phase with polarized layers.

Indeed, for very strong dipoles shifted towards the end ($\mu^* = 2.5, d^* = 0.75$, $\alpha = 76\%$) a bilayer crystalline structure with tetragonal in-plane ordering is achieved (Fig. 13). Now both order parameters ζ_1 and τ_2 are

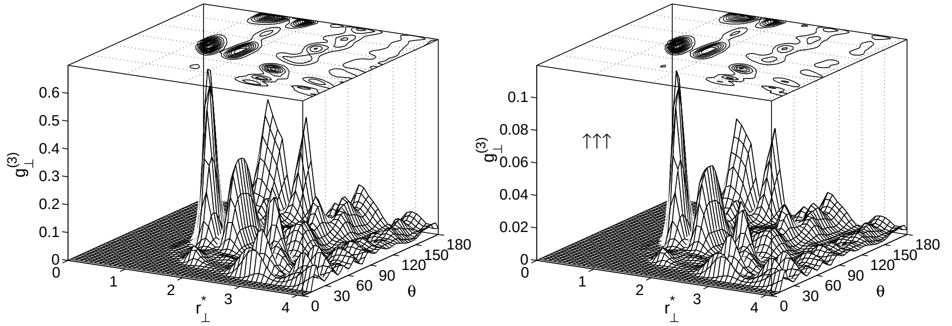

Fig. 11. The in-layer center of mass triplet distribution function $g_\perp^{(3)}(r_\perp^*, \theta, s_1 s_2 s_3)$ of polar, ideally oriented Gay–Berne system in the crystalline smectic phase of tetragonal symmetry: (a) — the total distribution function; (b) — the $s_1 s_2 s_3 = \uparrow\uparrow\uparrow$ distribution function. The dipolar strength and the dipole location are $\mu^* = 2$ and $d^* = 0.75$, respectively.

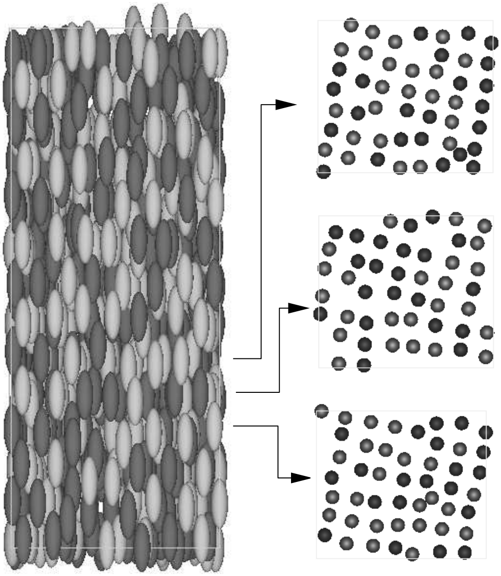

Fig. 12. Snapshot of the molecular configuration in crystalline smectic phase of tetragonal symmetry for $\mu^* = 2.0$ and $d^* = 0.75$. Dark molecules represent *up* orientation ($s = +1$) of the dipole moment; light ones are for $s = -1$.

nonzero and high, yielding $\zeta_1 = 0.89$ and $\tau_2 = 0.75$, which indicates that the antiferroelectric dipolar order is even stronger than the smectic ordering (see Table I). Thus, the crystalline structure that we discovered has similar dipolar ordering as the antiferroelectric smectic A_2.

TABLE I

Various phases resulting from Monte Carlo simulations in dependence on the location d^* and strength μ^* of the molecular dipole moments for $T^* = 2.8$ and $\rho^* = 0.335$. The meaning of symbols is: N (ideal nematic phase), A (smectic A phase), $S_{\mathrm{Cr}T}$ (crystalline smectic phase with dipolar disorder and transversal tetragonal lattice structure), CrA_2 (crystalline bilayer phase with transversal tetragonal lattice structure), $\tilde{A}$ (smectic $\tilde{A}$ phase, transversal domain structure). Also are given: dipolar order parameter ζ_1, smectic order parameter τ_1, hexagonal order parameter $\tau_\perp$ and hexagonal leading bond order parameter Ψ_6. Note that all quantities with asterisk are given in reduced units introduced in the appendix A.

$(d^*,$	$\mu^*)$	phase	ζ_1	τ_2	$\tau_\perp$	Ψ_6
(0,	0)	N	—	0.025	—	0.017
(0,	1.5)	S_A	0	0.11	—	—
(0,	2)	$S_B{}^1$	0	0.8	0.38^2, 0.23^3	0.69, 0.78^4
(0.75,	1.5)	$S_A{}^1$	0.065	0.35	—	—
(0.75,	2)	$S_{\mathrm{Cr}T}$	0.14	0.55	—	0.08
(0.75,	2.5)	CrA_2	0.89	0.75	—	—
(1,	2)	$\tilde{A}$	—	—	—	—

[1] See text for more details.

[2] In-layer value.

[3] Bulk value for ABAB stacking of layers.

[4] Value for $T^* = 2$.

The APDF (Fig. 14) also clearly reveals the bilayer structure: the peaks of $g_{||}^{(2)}(z, \uparrow\uparrow)$ and $g_{||}^{(2)}(z, \uparrow\downarrow)$ are shifted with respect to each other by one period. Interestingly, the axial *up–up* correlation are stronger than the *up–down* correlations. Also note that *up–down* correlations ($g_\perp^{(2)}(r_\perp, \uparrow\downarrow)$ in Fig. 15) are almost negligible within one smectic layer.

The crystalline structure is clearly of tetragonal symmetry, which is obvious from a snapshot of the molecular configuration, Fig. 13, and from the total in-layer triplet distribution function (Fig. 16).

For large shifts in the dipole location ($d^* = 1.0$) and $\mu^* = 2$ we recovered planar domains very similar to those reported by Berardi *et al.* [30] (Table II). As the present systems were too small to analyse quantitatively the $S_{\tilde{A}}$ configurations we postpone the analysis of these cases to our future publication.

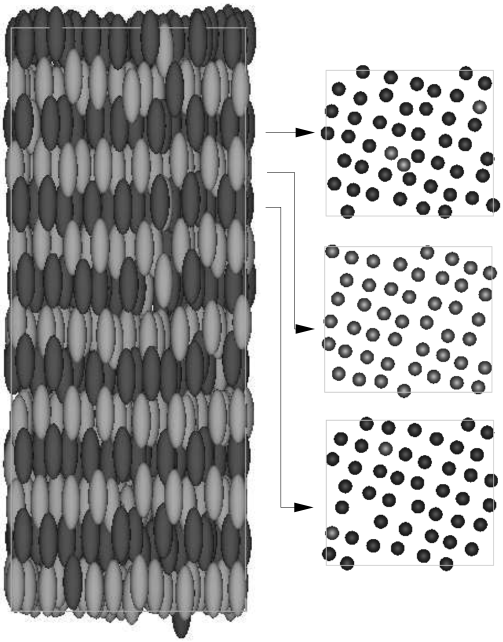

Fig. 13. Snapshot of the molecular configuration in crystalline smectic phase of tetragonal symmetry with polarized layers. Dark molecules represent *up* orientation ($s = +1$) of the dipole moment; light ones are for $s = -1$. The dipolar strength and the dipole location are $\mu^* = 2.0$ and $d^* = 0.75$, respectively.

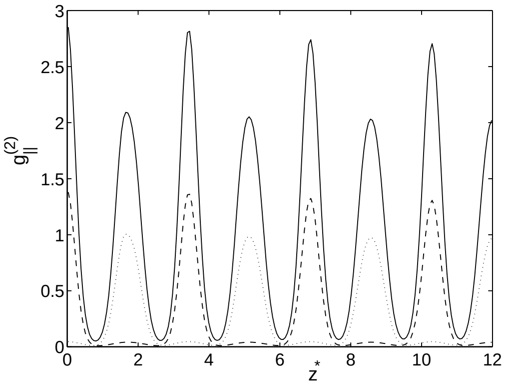

Fig. 14. The axial pair distribution function, $g_{||}^{(2)}(z^*, s_1 s_2)$, in the crystalline bilayer smectic phase. The solid line represents the dipole-averaged total distribution function $g_{||}^{(2)}(z^*)$, dashed line is for $s_1 s_2 =\uparrow\uparrow$, and dotted for $s_1 s_2 =\uparrow\downarrow$. The dipolar strength and the dipole location are $\mu^* = 2.5$ and $d^* = 0.75$, respectively.

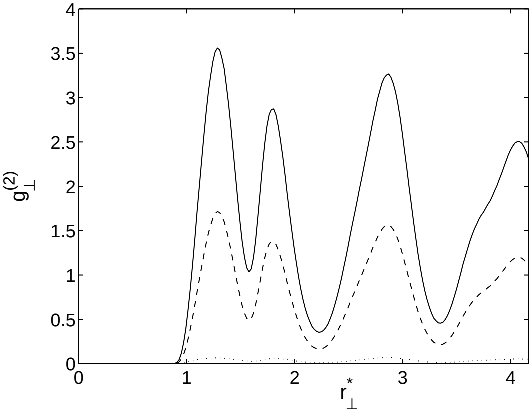

Fig. 15. The transversal pair distribution function, $g_\perp^{(2)}(r_\perp^*, s_1 s_2)$, in the crystalline bilayer smectic phase of polar molecules with $\mu^* = 2.5$ and $d^* = 0.75$. The continuous line represents the total distribution function $g_\perp^{(2)}(r_\perp^*)$ while dotted and dashed lines correspond to $s_1 s_2 = \uparrow\downarrow$ and $s_1 s_2 = \uparrow\uparrow$ cases, respectively.

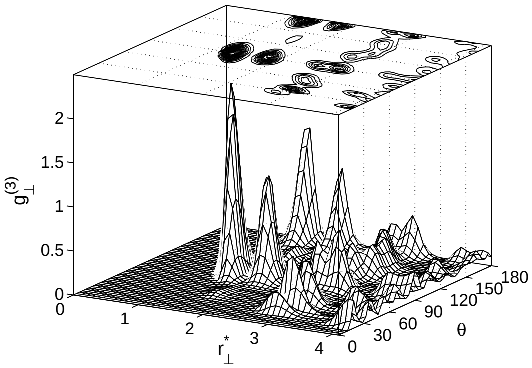

Fig. 16. The total in-layer center of mass triplet distribution function $g_\perp^{(3)}(r_\perp^*, \theta)$ in the crystalline bilayer smectic phase of polar molecules with $\mu^* = 2.5$ and $d^* = 0.75$.

5. Summary and conclusions

In this paper Monte Carlo simulations were performed for an ideally oriented dipolar Gay–Berne system, which models uniaxial ellipsoidal molecules with longitudinal, point dipole moment. The method employed in treating dipolar interactions was the Ewald summation technique [34,36]. The investigation has been directed towards the fulfillment of the three goals: *(i)* seek for new dipole-induced structures in the limit where nematic ordering is well established, *i.e.*, smectic and crystalline phases. To that aim we extended earlier works [25–31] by studying a Gay–Berne system with a different set of parameters. More specifically, we supplemented the simulations with central and terminal longitudinal dipole moments with those where the dipoles were positioned half way between the center and end of the molecule. Also we considered more possibilities for the dipole strength; *(ii)* study of large systems to gain more information about the structure of possible ordered phases and to avoid dependence on system size. Contrary to previous work [25–29] employing the reaction field method to treat dipolar interactions we used more reliable, but time consuming Ewald summation technique. Please note that simulations of liquid crystals using Evald method are scarce [30,31] and *apriori* it is not clear whether reaction field method is accurate for structures with long-range dipolar ordering, like the A_2 ordering; *(ii)* calculate and analyse various distribution functions, in particular the triplet ones, which, as far as we are aware of, have not been studied for polar liquid crystals so far. To make the analysis of the triplet distribution feasible we assumed the ideal nematic order approximation. This does not seem to be a severe approximation for structures where the nematic order is well established [17].

Our analysis clearly demonstrates the importance of triplet distribution functions for a proper understanding of dipolar organization in strongly polar liquid crystals. A restriction only to singlet and pair correlations misses structures derived from geometries representing frustration of dipolar interactions. This, in particular, is seen on going from central dipole moments ($d^* = 0$) to off-center dipoles positioned at $d^* = 0.75$, where the transformation from in-plane hexagonal to tetragonal ordering with indication on polymer-like correlations is observed.

By studying pair and triplet correlations we showed that the location and the strength of the dipole moment in the molecule has a profound effect on the short range in-layer molecular ordering and, consequently, also on the resulting phase behaviour. For example, the central dipoles ($d^* = 0$) may enhance local hexagonal order and the tendency of the system to form frustration-free polymer-like correlations. This, in turn, may stabilize the smectic A ordering (which is consistent with earlier results [7, 25, 26, 35]), smectic structures with nonvanishing hexatic order parameters and tetragonal structures with polarized layers.

For dipoles placed off-center ($d^* = 0.75$) the local hexagonal structure of the $d^* = 0$ case is abandoned by the system in favour of the tetragonal one. The latter seems much better suited to overcome the frustration effect by forming interdigitating layers. The level of interdigitation is such that the dipolar interactions of the neighbouring layers tend to minimize (and locally compensate). Again this could be visualized and quantified with the help of triplet correlation functions as shown in Figs. 10(a) and 10(b).

Upon systematic increase of the magnitude of the dipole moment at $d^* = 0.75$ we can observe an enhancement of short-range parallel dipolar correlations (see Figs. 10(c) and 11(b)). This indicates on the possibility of converting nonpolar layers into a polar bilayer crystalline structure of tetragonal symmetry, which we indeed observe for $\mu^* = 2.5$ (see Fig. 13). The dipolar organization in this structure appears very similar to that one found for the smectic A_2 phase. The last observation seems to hold in general. Namely, the local correlations of the triplet in-plane distribution function that enhance with increasing dipole moment usually correspond to long-range in-plane ordering found for stronger dipolar cases.

In conclusion, the striking changes in the local molecular organization as displayed by triplet correlations provide a wealth of information about the interplay between dipole position and its strength on liquid crystalline structures. The way in which the system deals with frustration also becomes apparent.

J.S. gratefully acknowlegdes his individual grant from the Alexander-von-Humboldt Stiftung. This research was supported by the EC PECO-Nis grant ERBCIPDCT940607 and by the Polish project KBN No. 2P03B21008. We also gratefully acknowledge the KBN computing grants (KBN/S2000/UJ/017/1998, KBN/SPP/UJ/003/1997) towards the cost of the ACK Cyfronet (Kraków) HP Exemplar S2000 and SPP1600/XA computers used to perform the Monte Carlo simulations.

Appendix A

Reduced units

The constants ϵ_0 and σ_0 of the GB potential (2) provide a natural length and energy scale for our problem. In terms of these constants all relevant physical quantities studied in this paper can be rendered dimensionless. The most often used reduced quantities (denoted by a star) are listed below:

- length: $l^* = l/\sigma_0$
- density: $\rho^* = \rho\,\sigma_0^3$
- energy: $E^* = E/\epsilon_0$
- temperature: $T^* = kT/\epsilon_0$
- dipole moment: $\mu^* = \mu\,(\epsilon_0\sigma_0^3)^{-1/2}$

Appendix B

Ewald sum

According to [11] the total dipolar energy can be expressed as

$$E = \frac{1}{2}\sum_{i\neq j}(\boldsymbol{\mu}_i\cdot\boldsymbol{\mu}_j)\,B(r_{ij}) - (\boldsymbol{\mu}_i\cdot\boldsymbol{r}_{ij})\,(\boldsymbol{\mu}_j\cdot\boldsymbol{r}_{ij})\,C(r_{ij})$$

$$+\frac{2\pi}{V}\sum_{\boldsymbol{k}\neq 0}\frac{\exp(-k^2/4\gamma^2)}{k^2}\,|F(\boldsymbol{k})|^2 - \frac{2\pi}{3}\,\frac{\gamma}{\sqrt{\pi}}\sum_{i=1}^{N}\mu_i^2$$

$$\frac{2\pi}{3V}\left|\sum_{i=1}\boldsymbol{\mu}_i\right|^2 .$$

In the expression above $\boldsymbol{k}$ denotes the reciprocal lattice vectors $\boldsymbol{k}=(2\pi n_x/L_x,\, 2\pi n_y/L_y,\, 2\pi n_z/L_z)$ (with $n_x,\, n_y,\, n_z = 0,..,n_{\max}$) and γ is a convergence parameter.

The functions $B(r_{ij})$ and $C(r_{ij})$ are defined as

$$B(r_{ij}) \overset{\text{def}}{=} \frac{\operatorname{erfc}(\gamma r_{ij})}{r_{ij}^3} + 2\,\frac{\gamma}{\sqrt{\pi}}\,\frac{\exp(-\gamma^2\, r_{ij}^2)}{r_{ij}^2}$$

and

$$C(r_{ij}) \overset{\text{def}}{=} 3\,\frac{\operatorname{erfc}(\gamma r_{ij})}{r_{ij}^5} + 2\,\frac{\gamma}{\sqrt{\pi}}\left(2\gamma^2 + \frac{3}{r_{ij}^2}\right)\frac{\exp(-\gamma^2\, r_{ij}^2)}{r_{ij}^2},$$

whereas

$$F(\boldsymbol{k}) \overset{\text{def}}{=} \sum_{i=1}^{N}(\boldsymbol{\mu}_i\cdot\boldsymbol{k})\,\exp(\mathrm{i}\,\boldsymbol{k}\cdot\boldsymbol{r}_i).$$

$\operatorname{erfc}(x)$ is the complementary error function:

$$\operatorname{erfc}(x) = \frac{2}{\sqrt{\pi}}\int_x^{\infty}\mathrm{d}t\, e^{-t^2}.$$

REFERENCES

[1] P.G. de Gennes, J. Prost, *The Physics of Liquid Crystals*, 2nd ed., Clarendon Press, Oxford 1993.

[2] G.W. Gray, J.W. Goodby, *Smectic Liquid Crystals. Textures and Structures*, Leonard Hill, Glasgow 1984.

[3] (a) G. Sigaud, F. Hardouin, M.F. Achard, H. Gasparoux, *J. Phys. Colloq.* **40**, C3-356 (1979); (b) A.M. Levelut, R.J. Tarento, F. Hardouin, M.F. Achard, G. Sigaud, *Phys. Rev.* **A24**, 2180 (1981); (c) F. Hardouin, *Physica* **A140**, 359 (1986); (d) J. Prost, P. Barois, *J. Chim. Phys.* **80**, 65 (1983).

[4] See *e.g.* (a) P.E. Cladis, *Phys. Rev. Lett.* **35**, 48 (1975); (b) L. Longa, W.H. de Jeu, *Phys. Rev.* **A26**, 1632 (1982); (c) L. Longa, W.H. de Jeu, *Phys. Rev.* **A28**, 2380 (1983); (d) L. Longa, Models of high-temperature liquid crystalline phases and of related phase transitions, Raport No 1454/PH (1989), Institute of Nuclear Physics, Kraków, Poland; (e) A.N. Berker, J.S. Walker, *Phys. Rev. Lett.* **47**, 1469 (1981).

[5] (a) C. Vega, S. Lago, *J. Chem. Phys.* **56**, 6727 (1994); (b) A.G. Vanakaras, D.J. Photinos, *Mol. Phys.* **85**, 1089 (1995).

[6] D.C. Williamson, F. del Rio, *J. Chem. Phys.* **107**, 9549 (1997).

[7] S.C. McGrother, G. Jackson, D.J. Photinos, *Mol. Phys.* **91**, 751 (1997).

[8] J.J. Weis, D. Levesque, G.J. Zarragoicoechea, *Phys. Rev. Lett.* **69**, 913 (1992).

[9] J.J. Weis, D. Levesque, G.J. Zarragoicoechea, *Mol. Phys.* **80**, 1077 (1993).

[10] D. Levesque, J.J. Weis, G.Z. Zarragoicoechea, *Phys. Rev.* **E47**, 496 (1993).

[11] J.J. Weis, D. Levesque, *Phys. Rev.* **E48**, 3728 (1993).

[12] S.C. McGrother, A. Gil-Villegas, G. Jackson, *J. Phys. Condens. Matter* **8**, 9649 (1996).

[13] A. Gil-Villegas, S.C. McGrother, G. Jackson, *Chem. Phys. Lett.* **269**, 441 (1997).

[14] J.G. Gay, B.J. Berne, *J. Chem. Phys.* **74**, 3316 (1981).

[15] E. de Miguel, L.F. Rull, M.K. Chalam, K.E. Gubbins, *Mol. Phys.* **71**, 1223 (1990).

[16] E. de Miguel, L.F. Rull, M.K. Chalam, K.E. Gubbins, F. van Swol *Mol. Phys.* **72**, 593 (1991).

[17] E. de Miguel, L.F. Rull, M.K. Chalam, K.E. Gubbins, *Mol. Phys.* **74**, 405 (1991).

[18] D.J. Adams, G.R. Luckhurst, R.W. Phippen, *Mol. Phys.* **61**, 1575 (1987).

[19] G.R. Luckhurst, R.A. Stephens, R.W. Phippen, *Liq. Cryst.* **8**, 451 (1990); G.R. Luckhurst, P.S.J. Simmonds, *Mol. Phys.* **80**, 233 (1993); A.P.J. Emerson, G.R. Luckhurst, S.G. Whatling, *Mol. Phys.* **82**, 113 (1994); R. Hashim, G.R. Luckhurst, S. Romano, *J. Chem. Soc. Faraday Trans.* **91**, 2141 (1995).

[20] M.A. Bates, G.R. Luckhurst, *J. Chem. Phys.* **110**, 7087 (1999).

[21] M.P. Allen, J.T. Brown, M.A. Warren, *J. Phys. Condens. Matter.* **8**, 9433 (1996); J.T. Brown, M.P. Allen, E. M. del Río, E de Miguel *Phys. Rev.* **E57**, 6685 (1998).

[22] R. Berardi, C. Fava, C. Zannoni, *Chem. Phys. Lett.* **236**, 462 (1995).

[23] G. La Penna, D. Catalino, C.A. Veracini, *J. Chem. Phys.* **105**, 7097 (1996).

[24] M.P. Neal, A.J. Parker, C.M. Care, *Mol. Phys.* **91**, 603 (1997).

[25] K. Satoh, S. Mita, S. Kondo, *Liq. Cryst.* **20**, 757 (1996).

[26] K. Satoh, S. Mita, S. Kondo, *Chem. Phys. Lett.* **255**, 99 (1996).

[27] K. Satoh, S. Mita, S. Kondo, *Mol. Cryst. Liq. Cryst.* **300**, 143 (1997).

[28] M. Houssa, A. Qualid, L.F. Rull, *Mol. Phys.* **94**, 439 (1998).

[29] M. Houssa, L.F. Rull, S.C. McGrother *J. Chem. Phys.* **109**, 9529 (1998).

[30] R. Berardi, S. Orlandi, C. Zannoni, *Chem. Phys. Lett.* **261**, 357 (1996).

[31] G. Cholewiak, J. Stelzer, L. Longa, *SPIE Int. Soc. Opt. Eng.* **3318**, 179 (1998).

[32] A.V. Zakharov, S. Romano *Phys. Rev.* **E58**, 7428 (1998).

[33] C.G. Gray, Y.S. Sainger, C.G. Joslin, P.T. Cummings, S. Goldman, *J. Chem. Phys.* **85**, 1502 (1986).

[34] M.P. Allen, D.J. Tildesley, *Computer Simulation of Liquids*, Clarendon Press, Oxford 1987.

[35] S.C. McGrother, G. Jackson, *Phys. Rev. Lett.* **76**, 4183 (1996).

[36] S.W. de Leeuw, J.W. Perram, E.R. Smith, *Proc. R. Soc. Lonon.* **A373**, 27 (1980).

[37] W.J. McNeil, W.G. Madden, A.D.J. Haymet, S.A. Rice, *J. Chem. Phys.* **78**, 388 (1983).

[38] M. Fushiki, *Mol. Phys.* **44**, 307 (1991).

[39] See *e.g.* J.P. Hansen, I.R. McDonald, *Theory of Simple Liquids*, 2$^{\text{nd}}$ edition, Academic Press, 1986.

[40] P.S. Pershan, *Structure of Liquid Crystal Phases*, World Scientific Lecture Notes in Physics, Vol. 23, World Scientific, Singapore 1988.

[41] (a) An excellent review of present status of density functional theory is given by J.P. Hansen, in: *Observation, Prediction and simulation of Phase Transitions in Complex Fluids*, M. Baus (ed.) Kluwer Academic Publishers, 1995, p. 167; (b) A.D.J. Haymet, D.W. Oxtoby, *J. Chem. Phys.* **84**, 1769 (1986); (c) J.L. Barret, J.P. Hansen, G. Pastore, *Phys. Rev. Lett.* **58**, 2075 (1988).